Journal of Solid State Chemistry 183 (2010) 1663–1669

Contents lists available at ScienceDirect

Journal of Solid State Chemistry

journal homepage: www.elsevier.com/locate/jssc

Moderate pressure synthesis of rare earth nickelate with metal–insulator transition using polymeric precursors

C. Napierala [a,d,*], C. Lepoittevin [b], M. Edely [c], L. Sauques [d], F. Giovanelli [a], P. Laffez [a], G. VanTedeloo [b]

[a] LEMA, Site de l'IUT de Blois, 3 Place Jean Jaurès, 41000 Blois, France
[b] EMAT, University of Antwerp, Groenenborgerlaan 171, 2020 Antwerpen, Belgique
[c] LPEC, Avenue Olivier Messaien, 72085 Le Mans Cedex 9, France
[d] DGA, 16bis Avenue Prieur de la Côte d'Or, 94116 Arcueil, France

ARTICLE INFO

Article history:
Received 30 June 2009
Received in revised form
7 April 2010
Accepted 13 April 2010
Available online 7 May 2010

Keywords:
Rare-earth nickelate
Infrared furtivity
Transmisssion electron microscopy
Applied physics
Thermochromism

ABSTRACT

Rare earth nickelates exhibit a reversible metal–semiconductor phase transition that is, in the infrared range, responsible for a thermo-optical contrast. The state of the art synthesis of these compounds usually requires high oxygen pressure to stabilize Ni in the oxidation state 3^+. In this work, using polymeric precursor associated with moderate pressure annealing, we show that it is possible to obtain fully oxidized rare earth nickelate with metal–insulator transition. Using thermogravimetric analysis, X-ray diffraction and transmission electronic microscopy we compare different samples synthesized at different oxygen pressures and demonstrate their structural similarity. Thermo-optical properties were measured, in the infrared range, using reflectance measurements and confirmed the metal–insulator transition at 60 °C in both samples.TEM observations lead to the conclusion that the structure commonly obtained at 175 bar is perfectly observed in the 20 bar sample without major structural defects. The two samples exhibit a thermochromic behavior and thermo-optical properties of the two samples are equivalent.

1. Introduction

Nowadays smart materials, whose one or more properties can be significantly changed in a controlled fashion by external stimuli, such as stress, temperature or electric field, find more and more industrial applications [1,2]. Among the smart materials, rare-earth nickelates, which exhibit a metal–insulator (MI) transition responsible for optical change in the infrared range, are one of the promising materials for thermochromic devices or infrared furtivity [3,4]. Compared to the other infrared switching materials like VO_2 [5] or (Sm,Ca)MnO_3 [6,7], rare-earth nickelates have a sharper transition, whose temperature can be easily adjusted by an appropriate choice of the rare earth. [3,8,9]. The main difficulty for its synthesis is the need for high oxygen pressure, which consequently frustrates large scale applications.

Metal–insulator transition in rare-earth nickelates (space group *Pbnm*) requires the nickel to adopt the Ni^{3+} valence state, which is normally accomplished at high temperatures and high pressures. For thermochromic applications, it is necessary to stabilize Ni^{3+} to get the oxygen stoichiometry in the $RNiO_3$ compounds and, consecutively, the optimum metal–insulator transition. An oxygen deficit strongly influences transport properties and consequently may induce changes in thermo-optical properties [10].

Among the different methods that have been developed to synthesize $RNiO_3$, only those including annealing pressure as high as 200 bar give samples with sharp MI transition, except the synthesis of this film using pulsed laser or chemical vapor deposition [11,12]. Other thin films techniques require high process annealing. The use of moderate annealing condition leads usually to poor semiconductive properties, without the expected MI transition [13].

Rare-earth nickelates exhibiting interesting properties were synthesized by Lacorre et al. [8] under 150–200 bar oxygen pressure at 1000 °C using nitrate precursors. More recently, Escote et al. [14] have prepared polycrystalline samples of $RNiO_3$ (R=Pr, Nd, Sm) through different routes (metal oxides mixture, hydroxide precipitation and sol–gel process). All powders obtained by the three different methods were heat-treated several times at 1000 °C and 70 bar oxygen pressure.

In this work, we have synthesized polycrystalline samples of $Nd_{0.3}Sm_{0.7}NiO_3$ using polymeric synthesis and post-annealing at 20 and 175 bar, respectively. This composition is selected because it leads to metal–insulator transition around room temperature. Our intent is to validate the polymeric route for synthesis of rare earth nickelate powder or ceramics by showing that annealing at moderate pressure (20 bar) leads to the same structural and physical properties as the standard annealing at 175 bar. For this

* Corresponding author at: LEMA, Site de l'IUT de Blois, 3 Place Jean Jaurès, 41000 Blois, France.
E-mail address: cecile.napierala@gmail.com (C. Napierala).

0022-4596/$ - see front matter © 2010 Elsevier Inc. All rights reserved.
doi:10.1016/j.jssc.2010.04.019

study, X-ray diffraction, thermogravimetric analysis and transmission electron microscopy were used for structure characterizations. For thermochromic property evaluation, infrared reflectivity measurements have been performed.

2. Experimental

2.1. Sample preparation

Polycrystalline samples of $Nd_{0.3}Sm_{0.7}NiO_3$ were prepared by a modified sol–gel method adapted from Douy [15] using NiO, Sm_2O_3 and Nd_2O_3 precursors. The oxides were dissolved in nitric acid, leading to the corresponding nitrate salts. Appropriate amounts of each solution were mixed in the stoichiometric ratio and citric acid was added as a chelating agent. At 80 °C, acrylamide and N–N′–methylenediacrylamide were added in order to form a three-dimensional gel. The resulting polyacrilamide gel was calcined at 300 °C for 2 h and then at 650 °C for 5 h in a furnace, producing a spongy material that turned into a dark gray fine powder after 12 h annealing at 700 °C. The samples were heat-treated twice at 790 °C under 175 and 20 bar oxygen pressure for 12 h.

2.2. Characterizations

Powder X-ray diffraction patterns were collected at room temperature on a Rigaku Miniflex diffractometer using Cu $K\alpha$ radiation ($\lambda = 1.5418$ Å). Diffraction pattern was recorded in the 2θ range 10–120° (step $\Delta\theta = 0.02°$). X-ray data analysis was performed through the Rietveld method using a pseudo-Voigt function.

Thermogravimetric analysis is used to determine the oxygen level in the structure by reducing the material under a flowing mixture of H_2 3%/Ar 20%/N_2. The thermogravimetric data were obtained on a Perkin Elmer TGA 7 thermogravimetric analyzer working at a heating rate of 1.5 °C min^{-1}. About 40 mg of the sample was used in this experiment.

Specimens for transmission electron microscopy observations were prepared by grinding the powder in ethanol and depositing a drop on a carbon coated copper grid. Selected area electron diffraction (ED) patterns were obtained using a Philips CM20 transmission electron microscope (double tilt ± 45°) operating at 200 kV. High-resolution electron microscopy (HREM) was carried out on a JEOL 4000EX microscope top-entry microscope (double tilt ± 20°) operating at 400 kV.

Thermochromic potentialities of each sample were measured at 5 and 100 °C and infrared reflectivity measurements with a Nicolet Magna 860 spectrophotometer equipped with an integrating sphere (Hemispherical Directional Reflectometer SOC 100) including the specular and diffuse parts of reflectivity. For this last measurement, 1 g of powder was pelletized under 12 ton (surface area DONNE LA SURFACE DU DISQUE)

3. Results

3.1. X-ray diffraction

X-ray diffraction experiments on the powder confirm for each treatment the synthesis of a single-phase material, showing only the derived-perovskite structure. All peaks were indexed with the

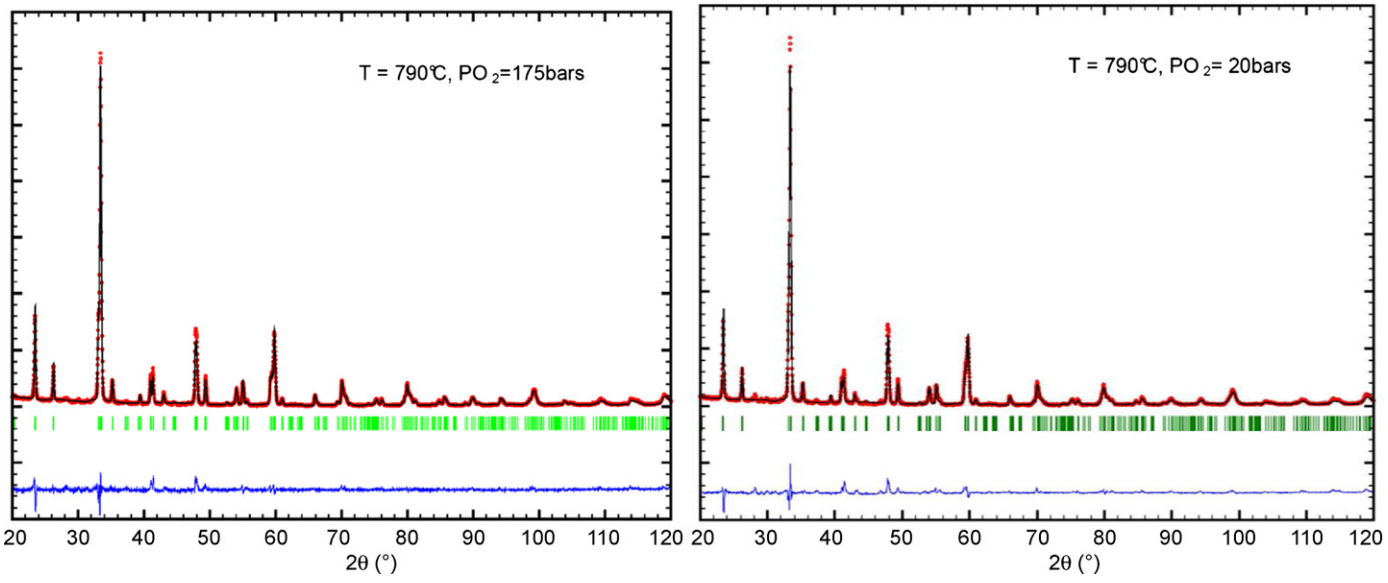

Fig. 1. X-ray diffraction patterns of $Nd_{0.3}Sm_{0.7}NiO_3$ samples annealed at 20 and 175 bar.

Table 1
Cell parameters, volume and nominal composition calculated from the thermogravimetric analysis for the $Nd_{0.3}Sm_{0.7}NiO_3$ compounds annealed at 175 or 20 bar of oxygen.

	Structure	Space Group	a (Å)	b (Å)	c (Å)	V (Å^3)	Weight loss (%)	$\delta_{calculated}$	Composition
$Nd_{0.3}Sm_{0.7}NiO_3$, $T = 790$ °C, $PO_2 = 175$ bar	Orthorhombic	*Pbnm*	$5.344 \pm 0.307 \times 10^{-3}$	$5.4136 \pm 0.336 \times 10^{-3}$	$7.5779 \pm 0.501 \times 10^{-3}$	219.23	9.32	0.02	$Nd_{0.3}Sm_{0.7}NiO_{2.98}$
$Nd_{0.3}Sm_{0.7}NiO_3$, $T = 790$ °C, $PO_2 = 20$ bar	Orthorhombic	*Pbnm*	$5.3502 \pm 0.386 \times 10^{-3}$	$5.4071 \pm 0.413 \times 10^{-3}$	$7.5822 \pm 0.615 \times 10^{-3}$	219.34	9.24	0.03	$Nd_{0.3}Sm_{0.7}NiO_{2.97}$

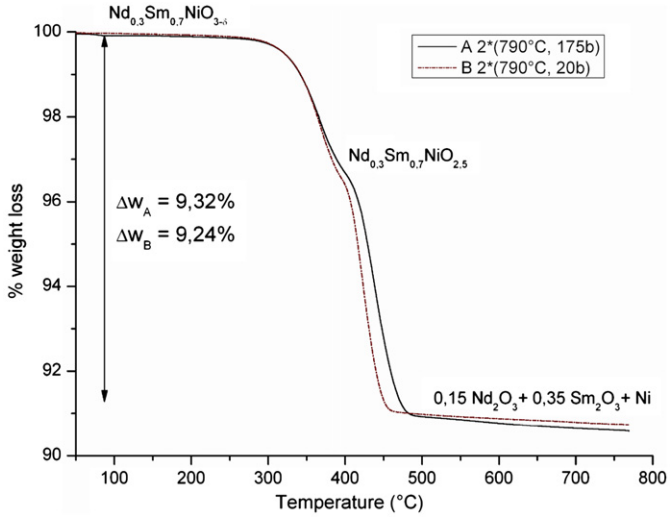

Fig. 2. Thermal analysis (TG) curves of $Nd_{0.3}Sm_{0.7}NiO_3$ samples annealed at 20 and 175 bar under reducing conditions (H_2/N_2flow).

orthorhombic distorted perovskite in *Pbnm* space group (Fig. 1). X-ray data analysis was performed through the Rietveld method and the refined cell parameters, presented in Table 1, are in good agreement with those found in literature [16,17]. We observe that both samples show the same cell parameters, whatever the annealing conditions, within the experimental precision.

3.2. Thermogravimetric analysis

Thermogravimetric analysis is used to evaluate oxygen rate in the structure by reducing $Nd_{0.3}Sm_{0.7}NiO_3$ under a H_2/N_2 flow. Fig. 2 shows the thermogravimetric profile for $Nd_{0.3}Sm_{0.7}NiO_3$ samples. The experiment suggests that the reduction process occurs through two consecutive steps ($Ni^{3+} \rightarrow Ni^{2+} \rightarrow Ni^0$) adapted from the equations in Falcon et al. [18] and Alonso et al. [19]:

$$Nd_{0.3}Sm_{0.7}NiO_{3-\delta} + (1/2-\delta)H_2 \rightarrow Nd_{0.3}Sm_{0.7}NiO_{2.5} + (1/2-\delta)H_2O$$

$$Nd_{0.3}Sm_{0.7}NiO_{2.5} + H_2 \rightarrow 0.15Nd_2O_3 + 0.35Sm_2O_3 + Ni + H_2O$$

For both compounds, the first decomposition step occurs at 350 °C and the second step at 450 °C. The decomposition process was confirmed by X-ray diffraction after each stage. Weight loss

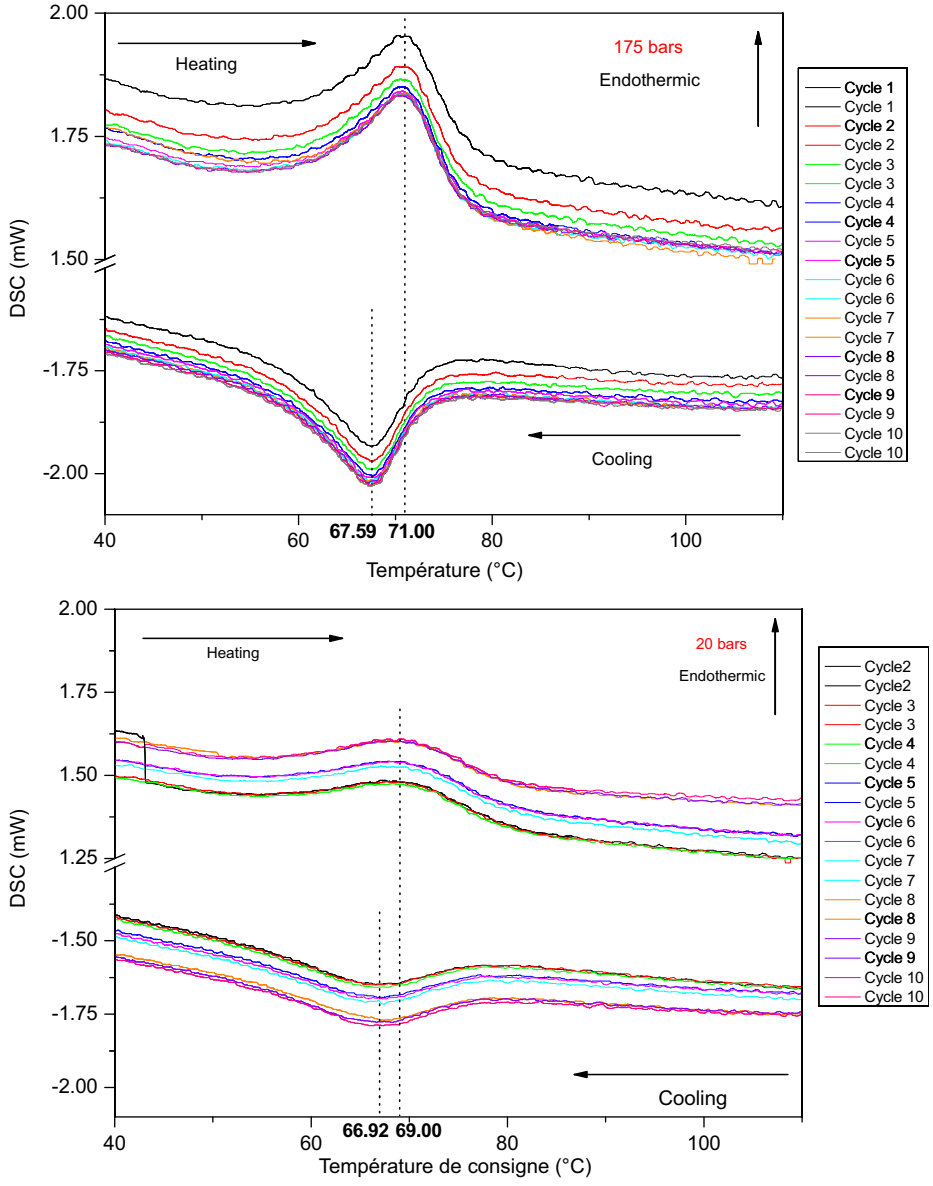

Fig. 3. DSC curves of $Nd_{0.3}Sm_{0.7}NiO_3$ samples annealed at 20 and 175 bar.

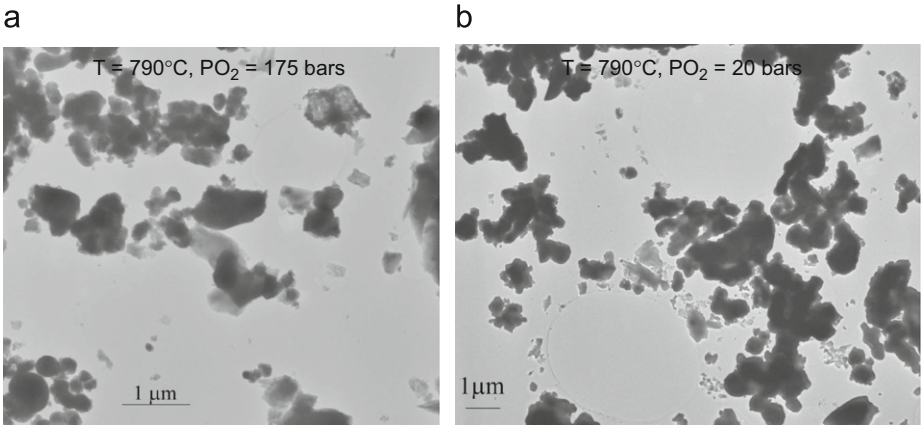

Fig. 4. Images of the two samples showing an inhomogeneous grain size with the formation of small agglomerated particles.

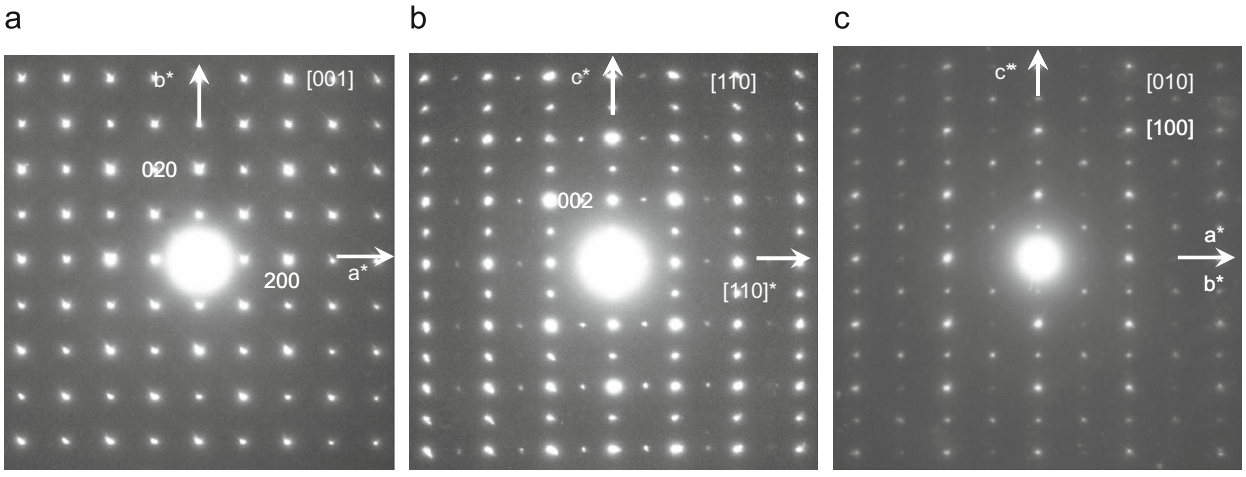

Fig. 5. Electron diffraction patterns of the $Nd_{0.3}Sm_{0.7}NiO_3$ samples.

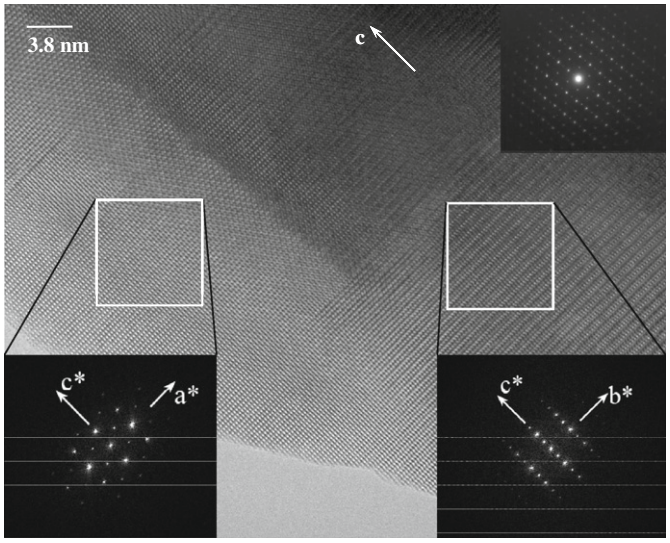

Fig. 6. HRTEM image showing a twinning in the $Nd_{0.3}Sm_{0.7}NiO_3$ sample.

and nominal composition of oxygen, calculated from the previous equations, are presented in Table 1. The calculated composition gives $Nd_{0.3}Sm_{0.7}NiO_{2.98}$ at 175 bar annealing and $Nd_{0.3}Sm_{0.7}NiO_{2.97}$ at 20 bar annealing (Fig. 3). Nominal oxygen compositions for both compounds are considered to be the same within the experimental error.

According to these first characterizations, both kinds of annealing allow obtaining of $Nd_{0.3}Sm_{0.7}NiO_3$ powders with similar structural properties. In order to check the influence of annealing pressure on these compounds, we performed a microstructural investigation using transmission electron microscopy.

3.3. Transmission electron microscopy

Few rare-earth nickelate characterizations by transmission electron microscopy are reported in literature. The only TEM studies on such compounds are the ones carried out on $NdNiO_3$ thin films deposited on silicon substrates in order to link sample preparation conditions to physical properties [20–22], and structural study at low temperature in order to characterize the structural transition [23]. In the present work, transmission electron microscopy is used to determine the influence of oxygen pressure on microstructure during post-annealing. Both samples exhibit an inhomogeneous grain size, small agglomerated particles forming aggregates of size ranging between 1 and 10 μm (Fig. 4a and b).

Fig. 5 shows typical ED patterns obtained for samples annealed either at 20 or 175 bar. The positions of reflections are characteristic of an orthorhombic lattice with $a \approx b \approx a_p\sqrt{2}$, $c \approx$

$2a_p$ (a_p=0.38 nm, the suffix p referring to the perovskite unit cell). Fig. 5b and c shows typical ED patterns illustrating twinning or 90° oriented domains resulting from geometric relationships between the unit cell parameters ($c=2d$[1 1 0] and $a=b$). Reconstruction of the reciprocal space was carried out by tilting around crystallographic axes, but determination of the conditions limiting the reflections was difficult to perform due to overlap of different twin domains. In order to solve this problem, HRTEM images showing oriented domains were recorded and fast Fourier transforms (FFTs) were performed on selected areas images. The HREM image in Fig. 6 was obtained on the 20 bar annealed sample and displays the [0 1 0] and [1 0 0] oriented areas with the corresponding FFTs. Combining these FFTs with the experimental [0 0 1] ED pattern (Fig. 5a), the conditions limiting the reflections become $0kl$: $k=2n$, $h0l$: $h+l=2n$, consistent with a *Pbnm* space group. After such preliminary microscopy results about the average structure, one may consider both samples are identical

However, considering that the aim of this microscopy work is to pick out the possibility that microstructural differences may appear, depending on the annealing condition, we investigated fine structure of the sample using high resolution imaging. We carefully looked for stacking defects, twinning, shearing or other defect commonly observed in the perovskite structure. According to the high resolution images recorded along different crystallographic axes on both materials ([0 0 1], [1 1 0], [0 1 0] and [1 0 0] zone axes), one can conclude that the structure commonly obtained at 175 bar is perfectly maintained on 20 bar sample without major structural defects; [0 0 1] and [0 1 0] high resolution images are presented as examples in Fig. 7 for both materials. Only very slight contrast differences can be observed in the [0 1 0] oriented images for the material prepared at 20 bar, leading us to perform FFTs on these small areas to understand if it is significantly correlated to a structural phenomenon (Fig. 8). It appears that a Fourier Transform realized inside or outside these areas gives the same diffraction pattern corresponding to the [0 1 0] zone axis, but at the interface one can observe diffuse scattering along the c^*-axis characteristic of local disorder. According to Ref. [24] the diffuse scattering may be related to oxygen vacancies created by lower oxygen pressure conditions in the 20 bar sample. However, the defects appear only time to time, and the average macroscopic structure seems independent of the annealing conditions.

3.4. Infrared measurement

Other studies have already described phonon behavior in rare-earth nickelates [25,26]. At low temperature, the spectra present insulator type reflectivity with well-defined phonon bands. Above the transition temperature, $Nd_{0.3}Sm_{0.7}NiO_3$ becomes metallic and the phonon bands are screened by delocalized mobile electrons.

To characterize optical reflectivity switching efficiency, it is usual to define a contrast factor in the 8–12 μm range, where

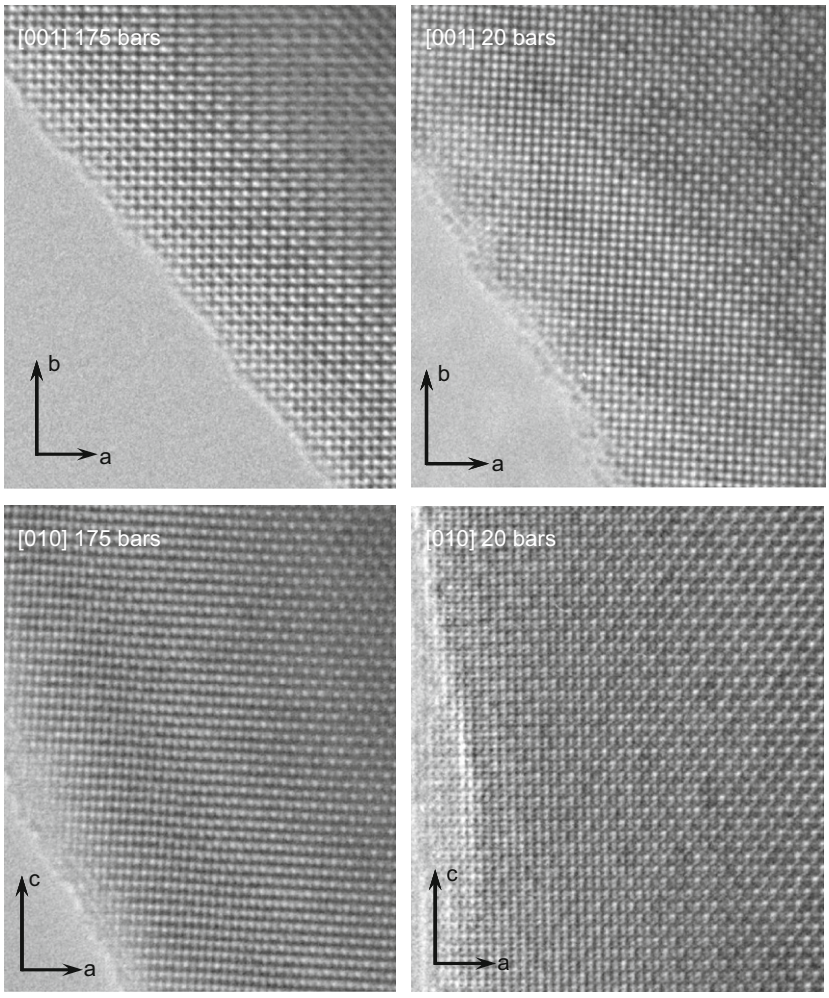

Fig. 7. HRTEM images of the two samples.

atmospheric transparency allows thermal detection (for more details, see [4,6]):

$$R(\Delta\lambda,T)=\frac{1}{\Delta\lambda}\int_{\lambda_1}^{\lambda_2}R(\lambda,T)d\lambda$$
$$\Delta R=R(\Delta\lambda,T_2)-R(\Delta\lambda,T_1) \quad (1)$$

Both samples show large change of IR reflectivity in band III with temperature and thus exhibit a thermochromic behavior (Figs. 8 and 9). The calculated infrared contrasts are 0.25 (25%) for the sample annealed at 175 bar and 0.2 (20%) for the 20 bar sample. Taking into account experimental error and surface state of each sample, these contrasts can be considered as equivalent for both samples. Such reflectivity data can be used for estimating spectral emissivity of the samples in the considered spectral band. The sample thickness causes transmittance to be null. Applying conservation principle of flux and Kirchoff's law, emissivity can be easily deduced as $\varepsilon_\lambda=1-\rho_\lambda$ (see Ref. [4] fore more details).

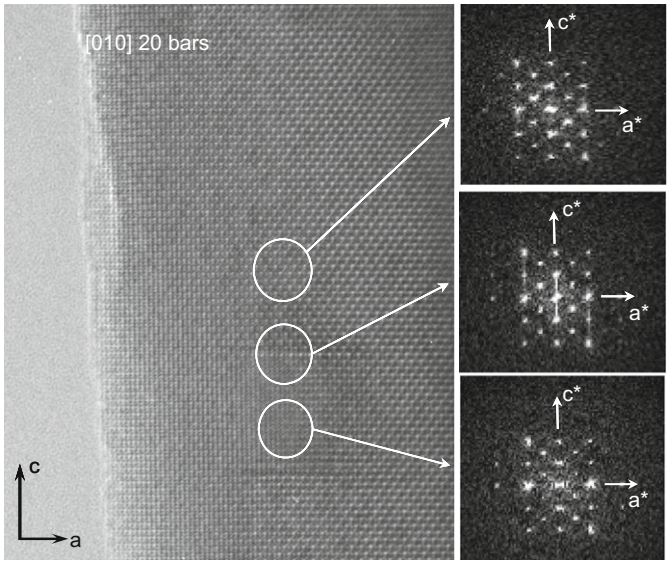

Fig. 8. Slight contrast differences can be observed in the [0 1 0] oriented images for the material prepared at 20 bar.

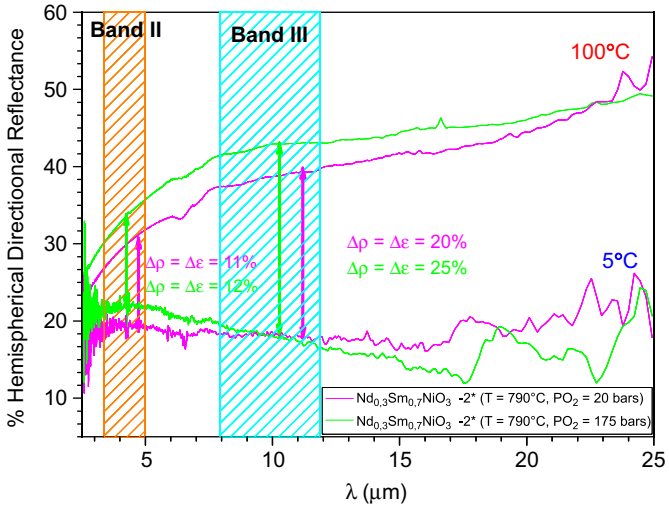

Fig. 9. Thermochromic behavior of $Nd_{0.3}Sm_{0.7}NiO_3$ samples annealed under 20 and 175 bar at 278 and 373 K.

Infrared emissivity for the sample annealed at 20 bar varied from 82% at 5 °C to 60% at 100 °C, whereas emissivity values for the sample synthesized at high pressure are 81% at 5 °C and 57% at 100 °C.

In the infrared-detection field (8–12 μm), a thermal imaging camera measures emittance of the object. This emittance, currently denoted by M, is the thermal power emitted by a unit surface in half space. This value is determined by

$$M=\varepsilon\sigma T^4 \quad (2)$$

where σ is the Stefan's constant ($5.67\times10^{-8}\,W\,m^{-2}\,K^{-4}$), ε and T are, respectively, the emissivity and real temperature of the sample (in K). Using the previous equation, emittance of each sample can be deduced. At 5 °C, emittance of each sample is $277.4\,W\,m^{-2}$ (20 bar) and $274.3\,W\,m^{-2}$ (175 bar). In a detection situation, the default value of emissivity is fixed and equal to one. Hence it allows determination of temperature observed by the infrared camera. The samples appear to be at −8.5 °C (20 bar) and −9.3 °C (175 bar) whereas the real temperature is 5 °C. Similarly the samples heated at 100 °C appear at 55.3 and 51.1 °C for, respectively, sample annealings under 20 and 175 bar.

4. Conclusions

In this study, we compare the influence of annealing conditions on microstructure and thermochromic behavior of $Nd_{0.3}Sm_{0.7}NiO_3$ powders. It appears that $Nd_{0.3}Sm_{0.7}NiO_3$ synthesized at 20 or 175 bar shows similar properties, with the same optical contrast and same metal–insulator transition. Oriented domains or twinnings are observed in both cases.

The decrease of oxygen pressure in the annealing process by nearly one decade for $Nd_{0.3}Sm_{0.7}NiO_3$ synthesis opens a large scale field application and allows considering the rare-earth nickelates as a good candidate for infrared coating or thermal detection.

References

[1] http://www.gentex.com.
[2] http://www.corning.com.
[3] F. Capon, P. Laffez, J.F. Bardeau, P. Simon, P. Lacorre, M. Zaghrioui, Applied Physics Letters 81 (2002) 619–621.
[4] C. Napierala, M. Edely, P. Laffez, L. Sauques, Optical Materials, 2009, available online at 〈doi:10.1016/j.optmat.2009.02.011〉.
[5] F. Guinneton, L. Sauques, J.C. Valmalette, F. Cros, J.R. Gavarri, Thin Solid Films 446 (2004) 287–295.
[6] P. Laffez, M. Zaghrioui, L. Reversat, P. Ruello, Applied Physics Letters 89 (2006) 081909.
[7] P. Laffez, C. Napierala, M. Zaghrioui, V.T. Phuoc, A. Hassini, M.R. Ammar, Applied Physics Letters 93 (2008) 151910.
[8] P. Lacorre, J.B. Torrance, J. Pannetier, A.I. Nazzal, P.W. Wang, T.C. Huang, Journal of Solid State Chemistry 91 (1991) 225–237.
[9] F. Capon, P. Ruello, J.F. Bardeau, P. Simon, P. Laffez, B. Dkhil, L. Reversat, K. Galicka, A. Ratuszna, Journal of Physics: Condensed Matter 17 (2005) 1137–1150.
[10] I.V. Nikulin, M.A. Novojilov, A.R. Kaul, A.F. Maiorova, S.N. Mudretsova, Materials Research Bulletin 39 (2004) 775–791.
[11] I.V. Nikulin, M.A. Novojilov, A.R. Kaul, S.N. Mudretsova, S.V. Kondrashov, Applied Physics Letters 76 (2000) 2041–2043.
[12] G. Catalan, R.M. Bowman, J.M. Gregg, Journal of Applied Physics 87 (2000) 606–608.
[13] J.D.G. Fernandes, D.M.A. Melo, L.B. Zinner, C.M. Salustiano, Z.R. Silva, C. Alves, J.A.P. da Costa, E. Longo, Journal of Alloys and Compounds 344 (2002) 157–160.
[14] M.T. Escote, A.M.L. Silva da, J.R. Matos, R.F. Jardim, Journal of Solid State Chemistry 151 (2000) 298–307.
[15] A. Douy, International Journal of Inorganic Materials 3 (2001) 699–707.
[16] G. Frand, O. Bohnke, P. Lacorre, J.L. Fourquet, A. Carre, B. Eid, J.G. Theobald, A. Gire, Journal of Solid State Chemistry 120 (1995) 157–163.
[17] A. Ambrosini, J.F. Hamet, B. Mercey, Applied Physics Letters 82 (2003) 727–729.
[18] H. Falcon, M.J. Martinez-Lope, J.A. Alonso, J.L.G. Fierro, Solid State Ionics 131 (2000) 237–248.

[19] J.A. Alonso, M.J. Lope Martinez, I. Rasines, Journal of Solid State Chemistry 116 (1995) 146–156.
[20] P. Laffez, R. Retoux, P. Boullay, M. Zaghrioui, P. Lacorre, G. van Tendeloo, The European Physical Journal—Applied Physics 12 (2000) 55–60.
[21] P. Laffez, M. Zaghrioui, R. Retoux, P. Lacorre, Journal of Magnetism and Magnetic Materials 211 (2000) 111–117.
[22] P. Laffez, O.I. Lebedev, P. Ruello, R. Desfeux, G. Banerjee, F. Capon, The European Physical Journal—Applied Physics 25 (2004) 25–31.
[23] M. Zaghrioui, A. Bulou, P. Lacorre, P. Laffez, Physical Review B 64 (2001) 081102(R).
[24] G. Van Tendeloo, S. Amelinckx, Phases Transitions 67 (1998) 101–135.
[25] M.A. Mroginski, N.E. Massa, H. Salva, J.A. Alonso, M.J. Martinez-Lope, Physical Review B 60 (1999) 5304–5311.
[26] T. Katsufuji, Y. Okimoto, T. Arimat, Y. Tokura, J.B. Torrance, Physical Review B 51 (1995) 4830–4835.